This document is downloaded from DR-NTU (https://dr.ntu.edu.sg)
Nanyang Technological University, Singapore.

Carbon–silica composite nanofiber membrane for high flux separation of water-in-oil emulsion – Performance study and fouling mechanism

Tai, Ming Hang; Juay, Jermyn; Leckie, James O.; Sun, Darren Delai

2015

Tai, M. H., Juay, J., Sun, D. D., & Leckie, J. O. (2015). Carbon–silica composite nanofiber membrane for high flux separation of water-in-oil emulsion – Performance study and fouling mechanism. Separation and Purification Technology, in press.

https://hdl.handle.net/10356/80871

https://doi.org/10.1016/j.seppur.2015.08.008

© 2015 Elsevier. This is the author created version of a work that has been peer reviewed and accepted for publication by Separation and Purification Technology, Elsevier. It incorporates referee’ s comments but changes resulting from the publishing process, such as copyediting, structural formatting, may not be reflected in this document. The published version is available at: [http://dx.doi.org/10.1016/j.seppur.2015.08.008].

Downloaded on 06 Dec 2023 02:52:57 SGT

Carbon-Silica Composite Nanofiber Membrane for High Flux Separation of Water-in-Oil Emulsion - Performance Study and Fouling Mechanism

Ming Hang Tai[a], Jermyn Juay[a], Darren D. Sun[a,*], James O. Leckie[b]

[a] *School of Civil and Environmental Engineering, Nanyang Technological University, Singapore 639798*

[b] *Department of Civil and Environmental Engineering, Stanford University, Stanford, California 94305-4020, United States*

[*] *Corresponding Author. Phone: (+65) 6790 627; Fax: (+65)-67910676; E-mail: ddsun@ntu.edu.sg (Darren D. Sun)*

Abstract

A flexible, hydrophobic and oleophilic carbon nanofiber membrane was prepared from electrospinning for cross-flow filtration of water-in-oil emulsion under various operating conditions. Experimental results show that the membrane has a high throughput of clean oil at low pressure. Furthermore, the membrane performance in terms of permeate flux was governed by the operating pressure and cross-flow velocity. The membrane has a water breakthrough pressure of 0.206 bar under constant cross-flow velocity. The investigation of membrane fouling mechanisms using pore blocking models and resistance model reveals that the membrane experiences either of external or internal fouling or a combination of both under different operating conditions. Using the contour plot analysis, it was suggested that the optimum operating conditions for the membrane to perform efficiently shall be at high cross-flow velocity and at low pressure (between 0.07 and 0.206 bar).

Keywords: Electrospinning, carbon nanofiber, superoleophilicity, membrane, oil-water separation.

1. Introduction

Oil is a hydrophobic liquid that is rich with hydrogen and carbon. It serves as an important energy resource and raw materials for various synthetic polymers and chemicals. There is a wide variety of oils that can be categorized based on the viscosity, volatility, toxicity and etc. For commercial use, oil needs to be processed to meet certain requirements such as high purity. This involves selective removal of unwanted components while concentrating the desired substances. One of the contaminants likely found in oil is water. Water can exist in oil in three states, namely free water, emulsified water and dissolved water. In some industries such as oil refinery and recovery industries, the existence of water in oil poses adverse effect to the oil performance and even to the machine component longevity. Therefore, purification of oil is important prior to further processing.

Traditional techniques used in oil-water separation involves chemical coalescence followed by gravity settling [1-2], air flotation [3-4] or flow through packed beds [5-6]. More advanced methodologies employ hierarchically micro and nano-structured materials such as zinc oxide rods [7], copper nanowires [8] and silica nanoparticles [9] to induce super selective wettability for high flux separation of oil-water emulsion. However, further study is required to examine their applicability at industrial scale. Recent development of membrane technology has opened up a new avenue for efficient processing of oil-water emulsion [10-15]. In theory, under pressurized condition, the wetting phase of the emulsion is driven through the membrane while retaining the non-wetting phase on the membrane surface.

The rejection efficiency is primarily dependent of the membrane pore size. A membrane with small pore size is able to reject smaller size of liquid droplets and vice versa. Generally, microfiltration and ultrafiltration membranes are two common types of membrane used for separation of oil and water [16-22]. Microfiltration membrane offers high flux but suffers from lower breakthrough pressure. In contrast, ultrafiltration membrane has tighter pore size and hence guarantees production of higher quality permeate. However, a higher operating pressure is required. Another factor affecting the rejection efficiency is the transmembrane pressure. When the applied pressure exceeds the liquid breakthrough pressure, they can be squeezed into and permeate through the membrane pore despite having larger size. Hence, the rejection efficiency is reduced. Taking these factors into consideration, a membrane that can produce a large quantity of high quality permeate at low operating pressure is highly favourable.

Electrospun fibrous membrane has been used as a free-standing filter media [23-25] or supporting substrate [26-27] to improve the permeate flux. Due to its interconnected open pore structure, the pores in the membrane are less likely to be entirely blocked by the particulates that have penetrated into the membrane. Hence, it is suitable to be used in liquid filtration under hydraulic pressure. When used as an independent filter media, the electrospun fibrous membrane has shown excellent liquid permeability at low applied pressure. This is advantageous because it is less prone to be membrane fouling under low pressure and the membrane life span can be extended.

While majority of the research focuses on treatment of oily water using hydrophilic polymeric membrane, less attention has been paid to the hydrophobic electrospun membrane for oil purification. Hence, the basic of this study objective is to evaluate the potential of electrospun carbon-based nanofibrous membrane as energy efficient and high flux oil-water separator. In this paper, the membrane performance and its fouling mechanisms will be discussed based on the fouling and resistance models. Lastly, an optimum operating condition is suggested.

2. Membrane Fouling Theory and Models

To identify the fouling mechanism, the resistance model derived from Darcy's law has been developed. The resistance model is expressed as

$$J = \frac{\Delta P}{\mu_o(R_t)} = \frac{\Delta P}{\mu_o(R_m + R_c)} \quad (1)$$

which can be rearranged into

$$R_t = \frac{\Delta P}{\mu_o J} \quad (2)$$

where J is the permeate flux, ΔP transmembrane pressure, μ_o the solution viscosity, R_t total resistance to flow, R_m the inherent membrane resistance and R_c the cake fouling. As seen, R_t is a total of R_m and R_c. The increase in R_m over time is due to the internal fouling that occurs in the internal pore structure of the membrane whereas the formation of cake layer is responsible for the increase in R_c. Both

standard blocking and complete blocking account for the internal fouling. On the other hand, external fouling is due to the formation of cake layer on membrane surface.

For standard blocking model, it is assumed that the foulants deposited evenly along the pore wall such that the pore diameter is reduced due to constriction in pore diameter while the number of pores is remained constant [28]. These assumptions yield the following expressions

$$\frac{t}{V} = K_1 t + \frac{1}{Q_o} \qquad (3)$$

where t is operation time, V the accumulated permeate volume, K_1 the standard blocking constant, Q_o the initial permeate flow rate. The value of initial flow rate and the constant, K_1 can be determined by plotting t/V versus t using experimental data. The standard blocking model can also be written in terms of membrane resistance as a function of time:

$$R_m = R_{mo}(1 + K_1 Q_o t)^2 \qquad (4)$$

where R_{mo} is initial membrane resistance. From equation (4), one can see that the resistance increases over time with an increasing slope and the curve produced from plotting the resistance versus time is concave up.

Assuming that the pore diameter is constant and the number of clogged pores increases with the permeation volume, the flow rate described by pore blocking model can be estimated using the following equation [28]:

$$Q = Q_o - K_2 V \quad (5)$$

where K_2 is the pore blocking constant. The value of Q_o and K_2 can be determined by plotting Q versus V. The expression in term of membrane resistance for pore blocking model is as follow:

$$R_m = R_{mo} e^{(K_3 t)} \quad (6)$$

The membrane resistance increases exponentially over time with an increasing slope. The plot of resistance against time produces a curve that is concave up.

The resistance to flow can also be contributed by the formation of cake due to the accumulation of rejected foulants on membrane surface. The membrane is fouled externally in this case. For external fouling, the membrane resistance is constant whereas the cake resistance increases with the time due to the accumulation of rejected foulants. This yields the following equation [28]:

$$\frac{t}{V} = K_3 V + \frac{1}{Q_o} \quad (7)$$

where K_3 is cake filtration constant. In terms of total resistance, the cake filtration model can be expressed as

$$R_{tot} = R_{mo}(1 + 4tK_3Q_o^2)^{0.5} \quad (8)$$

Like internal fouling model, the resistance increases with time. However, the changing pattern is a decreasing slope and the curve is concave down. In short, internal fouling model is characterized by an increasing slope while external fouling model has a decreasing slope. Therefore, by looking at the characteristic slope (concave up and down, increasing or decreasing slope) in a total resistance curve, one can readily identify the fouling mechanism.

3. Experimental

3.1 Preparation of Electrospun SiO_2-Carbon Composite Nanofibers.

The SiO_2-Carbon Composite Nanofibers was prepared according to Tai et al [29]. Briefly, polyacrylonitrile (PAN, M.W.=150000 g/mol, 7 wt%) and tetraethyl orthosilicate (TEOS, 0.5 wt%) was mixed with a mixture solvent of dimethylformamide (DMF)/acetic acid (volume ratio of 15/1). The precursor solution was then heated in water bath at 60°C for 30 min before it was used for electrospinning. The electrospinning was performed at room temperature in a closed chamber where the electric field strength was sustained at approximately 0.6-0.8 kV/cm. The tip-collector distance was kept at 20 cm. To retard the hydrolysis of precursor, N_2 was purged from the side of spinneret during the electrospinning. At a solution feeding rate of 9-10 μl/min, 11-15 hours were required to electrospin the

membrane. Subsequently, the collected non-woven fibrous assembly was oxidatively stabilized at 280°C for 2 hours followed by carbonization at 900°C in N_2 for another 2 hours.

3.2 Membrane Pore Size Determination

The pore size of the as-fabricated membrane was determined by a capillary flow porometer (CFP 1500A, Porous Material. Inc. (PMI), Singapore). The method used is bubble point analysis which is based on the fact that the pressure required to force an air bubble through the pore is inversely proportionally to the pore size. Hence, under wetting condition, the pore size can be determined from the pressure necessary to push water out of the pore.

Prior to analysis, the membrane was pre-wetted with Galwick fluid (surface tension = 15.9 dynes/cm). The measurement was performed in a dead-end cell where the wetted membrane was placed onto a filter holder that was connected to a source of regulated pressure. The pressure on the membrane was then increased stepwise while giving a 10 min stablization time after each 14 kPa increment. 3 identical membrane samples were analyzed and the average values were obtained.

3.3 Preparation of Water-in-Oil Emulsion

Water-in-hexadecane emulsion was used as feed solution. A specified amount of deionized water was added into hexadecane (density = 0.77g/ml) to make 1% water-emusified hexadecane. No surfactant was added in the preparation. The mixture then went through low-intensity ultrasonication in a water bath for 5 mins under mild mechanical mixing to form milky emulsion. The water-in-oil droplet sizes were observed under optical microscope.

3.4 Cross-flow Microfiltration of Water-in-Oil Emulsion

Electrospun carbon-silica composite nanofiber membranes after pre-treated with silicone coating via chemical vapor deposition were employed in this experiment. Prior to introduction into the membrane module, the membrane were cut into a shape that fits the membrane module. It is noteworthy that a pristine CNF membrane is very vulnerable to cutting and readily causes cracks. The cracks should be avoided because it adversely affects the filtration performance by lowering down the membrane rejection efficiency and giving inaccurate permeate flux. On the contrary, a carbon-silica nanofiber membrane is flexible and is more tolerable to some physical processing. Furthermore, the carbon-silica nanofiber membrane with enhanced toughness is more well-adapted to higher pressure condition.

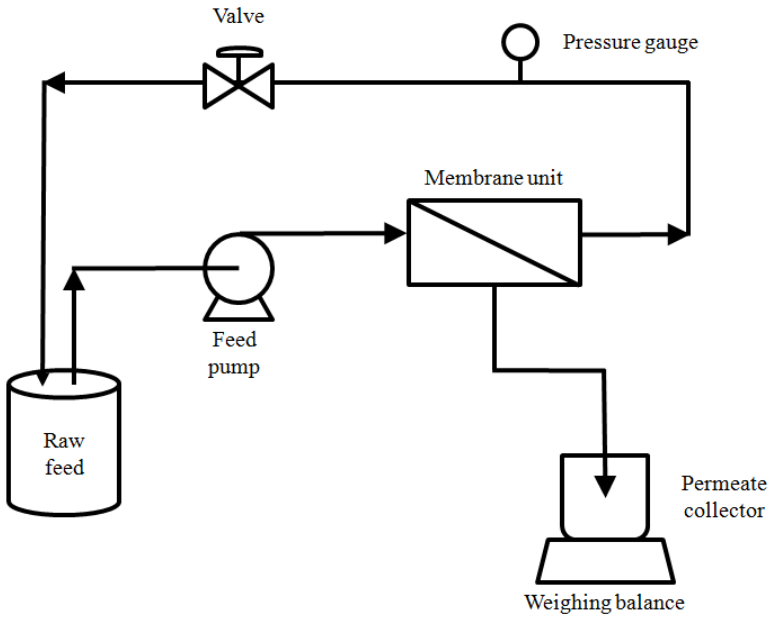

Figure 1. Schematic diagram of experimental setup for cross-flow microfiltration experiment.

The apparatus constructed for the cross-flow filtration experiment is shown schematically in Figure 1. A gear recirculation pump (Cole-Parmer) was used to circulate the feed emulsion from a feed tank into a membrane module unit. A pressure reading gauge was fitted at the outlet (retentate side) of the module unit to monitor the transmembrane pressure. The transmembrane pressure was adjusted through throttling the valve. By doing so, a back-pressure could be generated to the outlet of the membrane unit. The cross-flow velocity was determined by taking the feed flowing rate at the applied pressure over the cross-sectional area of the feed channel spacer. Both the permeate and retentate were pumped back to the feed tank. For permeate flux measurement, the permeate was collected in a beaker and weighed on a digital balance every 5 mins. The permeate collection time ranged between 20s and 60s. After that, the permeate was immediately transferred to the feed tank for recirculation. To avoid gradual depletion of water concentration due to the coalescence and deposition on the side of tank, the feed solution was replenished with stable emulsion every 5 mins.

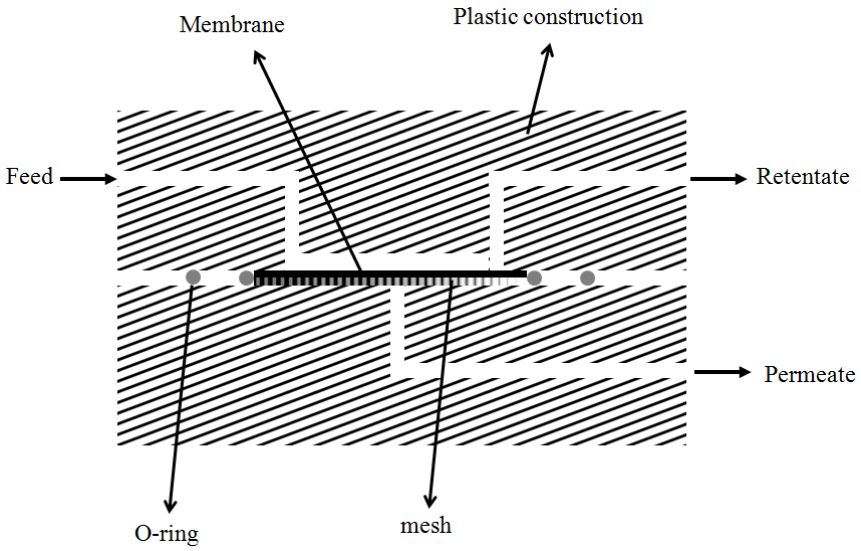

Figure 2. Schematic diagram of a membrane module unit for cross-flow filtration.

The membrane module unit is constructed by two pieces of machined rectangular plastic constructions, each has a dimension of 14 x 12 x 2.5 cm. The upper section includes a rectangular feed flow channel where filtration process was performed. The lower section is used to hold the membrane. A hole with 0.5 cm diameter is drilled at the lower section so that the filtrate that permeate through the membrane can flow to the collecting outlet. To assembly, the membrane is first wetted before it is mounted and sealed with O ring gaskets. A permeate spacer (polymeric mesh) of the same size is placed underneath the membrane. The upper and lower sections is secured by 6 tie bolts. During the operation, the membrane has an effective filtration area of 23.76 cm^2 or 0.002376 m^2. The design of the membrane module unit is illustrated in Figure 2.

Before each experiment, the membrane was pre-coated with silicone oil via chemical vapor deposition. The coating was performed in oil bath at 140°C for an hour to increase the membrane's hydrophobicity. Prior to permeate flux measurement, the membrane was pre-filtered with pure hexadecane for 60 mins to complete membrane compaction which may affect the membrane performance. This followed by filtration of water-in-hexadecane emulsion for another 150 mins. For each run, the transmembrane pressure and cross-flow velocity were varied to study their effect to the membrane performance respectively. The permeate was collected at a time interval of 5 mins and the mass of the collected permeate was measured on a digital balance (Shimadzu, UX4200H). All the experiments were conducted at temperature of 21-22°C.

4. Results and discussion

4.1 Characterization of Carbon-Silica Nanofiber Membrane

The as-fabricated carbon-silica nanofiber membrane used in the experiment has an average fiber diameter of 481 ± 57 nm. The bubble point analysis reveals that the membrane has a mean pore diameter of 1.203 ±0.251 μm with the smallest pore size being 0.902 ±0.182 μm. Figure 3 shows the representative pore size distribution of the membrane.

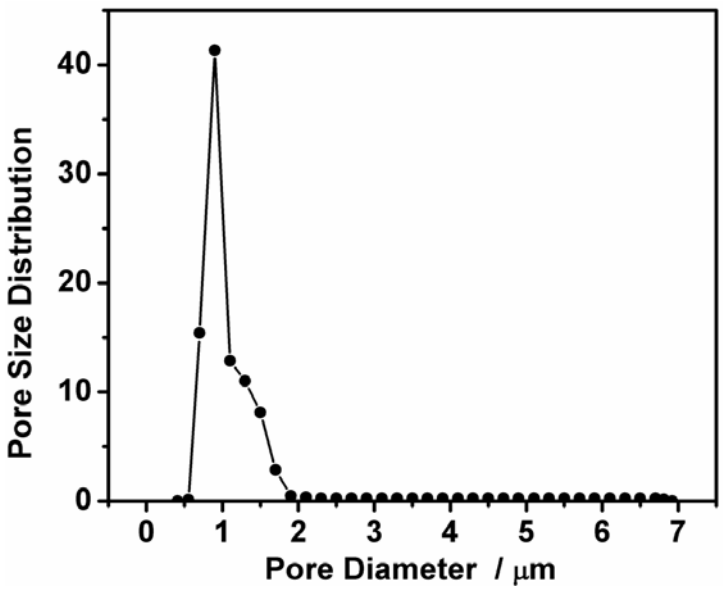

Figure 3. Representative Pore Size Distribution of Silica-Carbon Nanofiber Membrane.

4.2 Pure Oil Flux

The permeation flux of pure hexadecane at various operating pressures is shown in Figure 4. As seen, the flux was increased with increasing applied pressure in a nonlinear manner. It appeared that the flux is approaching a plateau at higher

pressure. Due to its unique characteristics of high porosity and interconnected open pore structure, the electrospun carbon-silica nanofiber membrane is capable of producing a large amount of oil at very low pressure. For instance, a high flux of 2481 L/m^2-hr could be readily achieved at a pressure of 0.07 bar which is equivalent to 35961 L/m^2-hr-bar. The discussion in the later section shows that the electrospun membranes could achieve a flux greater than 100 L/m^2-hr for water-in-oil emulsions. This is higher than the other reported membranes which are in different structures [17,30,31,32] and materials [33]. For example, under its optimum operating conditions, a hydrophobic polytetrafluoroethylene (PTFE) membrane is only capable of producing a permeate flux smaller than 100 L/m^2-hr [32]. Such high oil throughput makes the electrospun membrane a potential candidate for energy efficient treatment of waste water-in-oil emulsion.

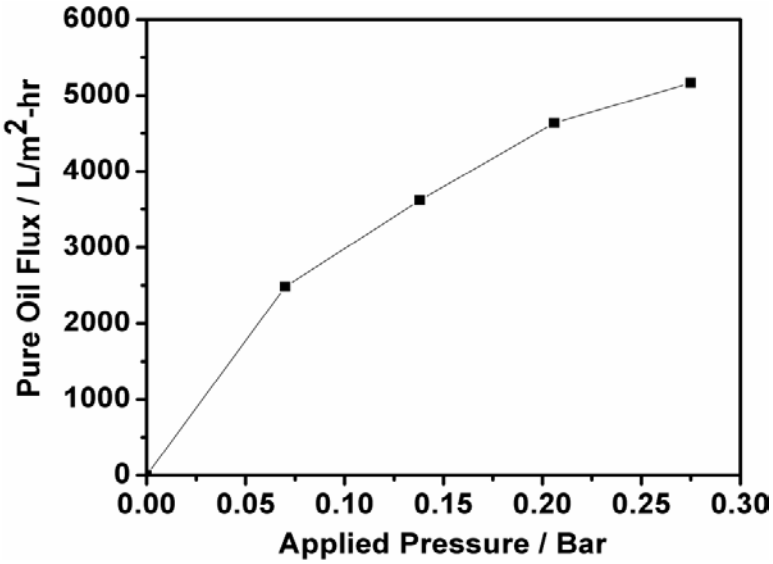

Figure 4. Pure oil flux as a function of operating pressure.

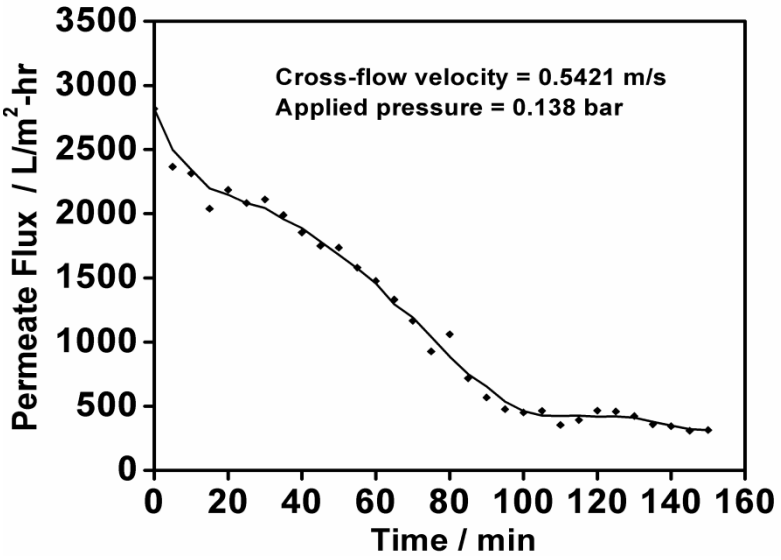

Figure 5. Typical Oil Flux Model of An Electrospun Nanofiber Membrane.

Figure 5 shows the representative filtration model of an electrospun nanofiber membrane. It is observed that the flux declines rapidly with operation time. This followed by a gradual flux decline before it reaches its equilibrium state. This filtration model is similar to that of the colloidal solution [34]. However, depending on the operating conditions including cross-flow velocity and applied pressure, the rate of flux decline, initial flux, rejection efficiency and the final flux will vary. These factors have direct impact to the performance of the electrospun membrane.

4.3 Effect of Applied Pressure on Permeate Flux

Figure 6 shows variation of the initial permeate flux at applied pressure from 0.07 to 0.206 bar when water-in-oil emulsion was used. It can be clearly seen that the initial flux increased with increasing applied pressure. However, a different trend was observed when it comes to the final flux which is measured at the end of the runs. As seen in Figure 7, the permeate flux was reduced as the pressure was

increased to 0.138 bar. However, the flux was bounced back as pressure was further increased to 0.275 bar, reaching a value of 1839 L/m^2-hr. Obviously, the pressure has both positive and negative effect on the permeate flux which can be explained from the aspect of breakthrough pressure.

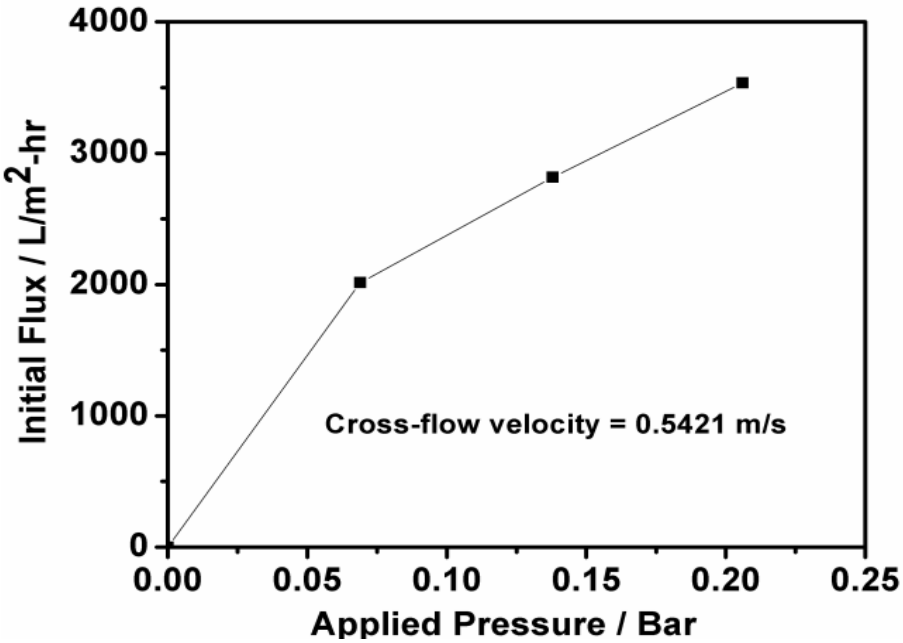

Figure 6. Initial Oil Flux Over A Range of Applied Pressure Under Constant Cross-Flow Velocity of 0.5421 ms^{-1}.

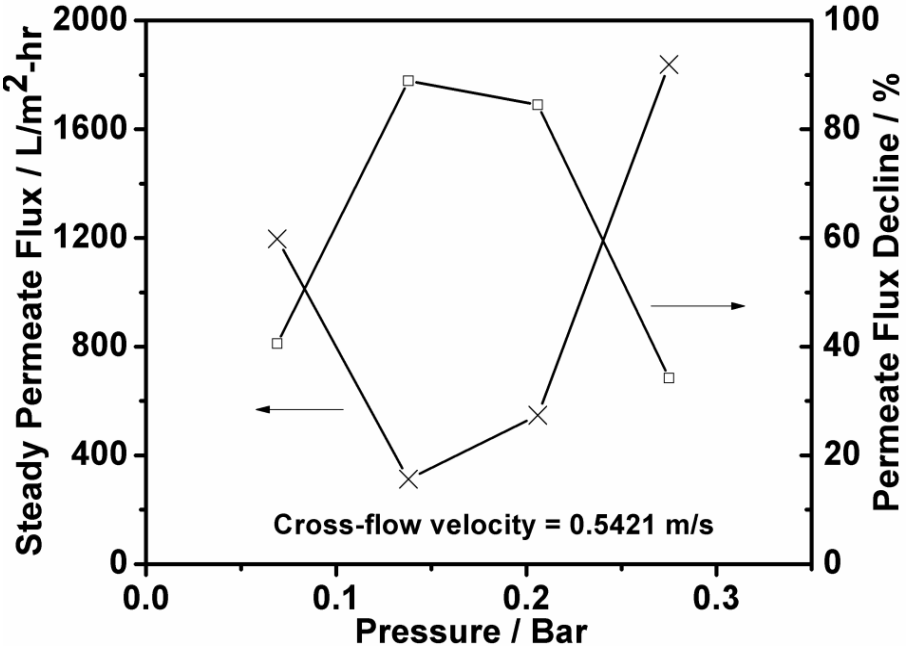

Figure 7. The Variation of Final Permeate Flux and the Corresponding Decline in Permeate Flux as a Function of Applied Pressure under constant Cross-flow Velocity of 0.5421 m/s.

A breakthrough pressure is defined as the maximum allowable pressure of a solute before it permeates through the membrane. As the pressure was lower than 0.138 bar, increasing the pressure decreased the permeate flux because more emulsified water-hexadecane droplets accumulated on the membrane surface due to increased build-up of concentration polarization layer. This effect is likely to squeeze the emulsion droplet into the membrane pore and eventually led to pore blocking that caused the flux to decline. Hence, the flux decline percentage was high. However, at pressure equal to and beyond 0.206 bar, increasing the pressure increased the flux due to the fact that the water-hexadecane droplets permeated through the membrane as observed during the experiments. In this pressure region, the percentage of flux decline was reduced at the expense of water rejection efficiency. To sustain

production of high quality permeate, the membrane shall be operated at a pressure below 0.206 bar which is also the breakthrough pressure for hexadecane in this case.

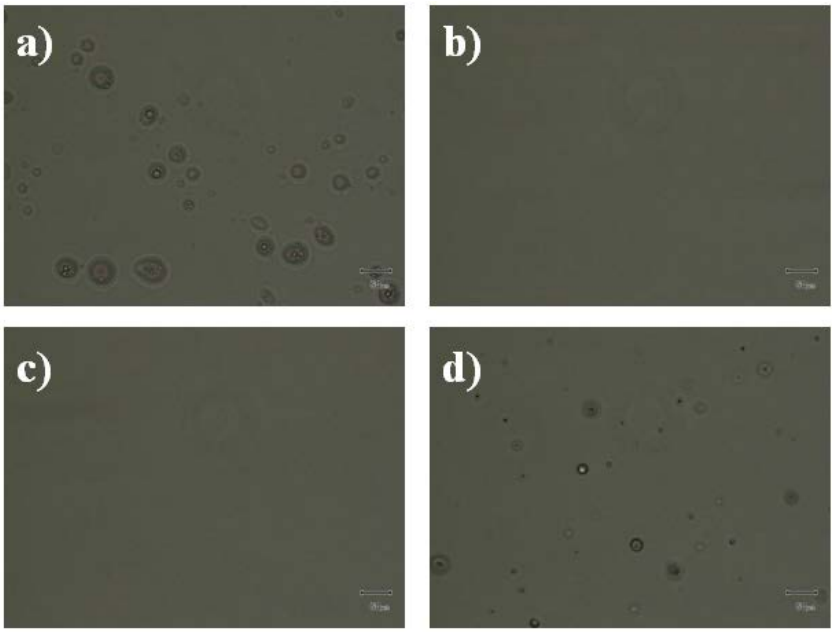

Figure 8. Representative Optical Microscopy Image of a) Feed water-in-oil Emulsion and the Permeate Collected at b) 0.07 bar c) 0.138 bar and d) 0.275 bar.

Figure 8 shows the representative optical microscopy images of feed emulsion and permeates collected at different operating pressures. It is clearly seen that the as-prepared feed emulsion contains water-oil emulsion droplets of different sizes. After membrane filtration, no droplets were observed in the collected permeate except for that collected at 0.275 bar. It was observed that at 0.206 and 0.275 bars, emulsion droplets broke through the membrane and flowed into the permeate. Hence, It is postulated that the permeate collected at 0.206 bar also contains emulsion droplets. However, it is worth to note that the breakthrough pressure for emulsion droplets may vary with shear rate, surface tension coefficient and droplet

viscosity. It is reported that at a fixed shear rate, the breakthrough pressure is higher for more viscous droplets [35].

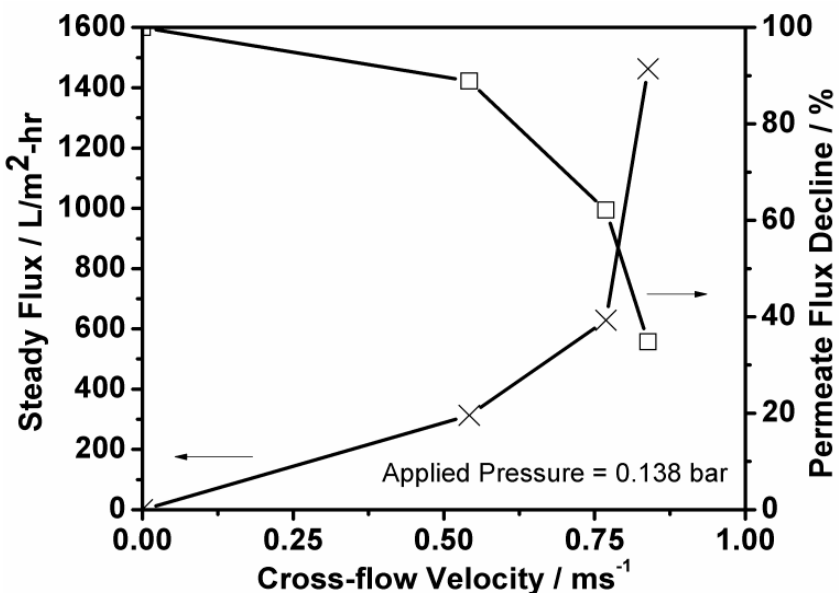

Figure 9. The Variation of Final Permeate Flux and the Corresponding Decline in Permeate Flux as a Function of Cross-flow Velocity under constant Applied Pressure of 0.138 bar.

4.4 Effect of Cross-flow Velocity on Permeate Flux

The effect of cross-flow velocity varied from 0 to 0.8387 m/s to final flux under a constant pressure of 0.138 bar is shown in Figure 9. The results showed that higher cross-flow velocity gave rise to higher final permeate flux and therefore lower percentage in flux decline. This phenomenon could be explained by the increase in shear rate which is expressed as $S = 4Q/\pi r^3$, where Q is cross-flow volumetric rate(m^3/s), and r the inner radius of pipe (m). As cross-flow velocity was varied from 0 to 0.8387 m/s, the shear rate was increased from 0 to 2236.4 /s. This made

the shear force sufficient to scour off the water-hexadecane droplets accumulated on the membrane surface. The retained water-hexadecane droplets could form a gel layer that added up additional hydraulic resistance to the total resistance and hence induced a pressure drop. The difference in flux decline observed in Figure 9 was a result of different cake layer thickness. At high shear rate, the gel layer thickness was kept minimum that the hydraulic resistance did not cause a significant pressure drop. Therefore, a higher final flux was resulted. A 34.8% flux decline was achieved when the cross-flow velocity was maintained at 0.8387 m/s. It is noted that cross-flow velocity operated beyond 0.8387 m/s is not feasible because the corresponding minimum pressure required is above 0.138 bar which exceeds the hexadecane breakthrough pressure.

4.5 Membrane Fouling Characterization

To characterize the fouling mechanism, the internal and external fouling models derived from Darcy's law are employed. For internal fouling model, the corresponding resistance curve increases with an increasing slope over the time whereas external fouling model yields a curve with a decreasing slope. This offers a simple yet straightforward mean of identifying the membrane fouling mechanism.

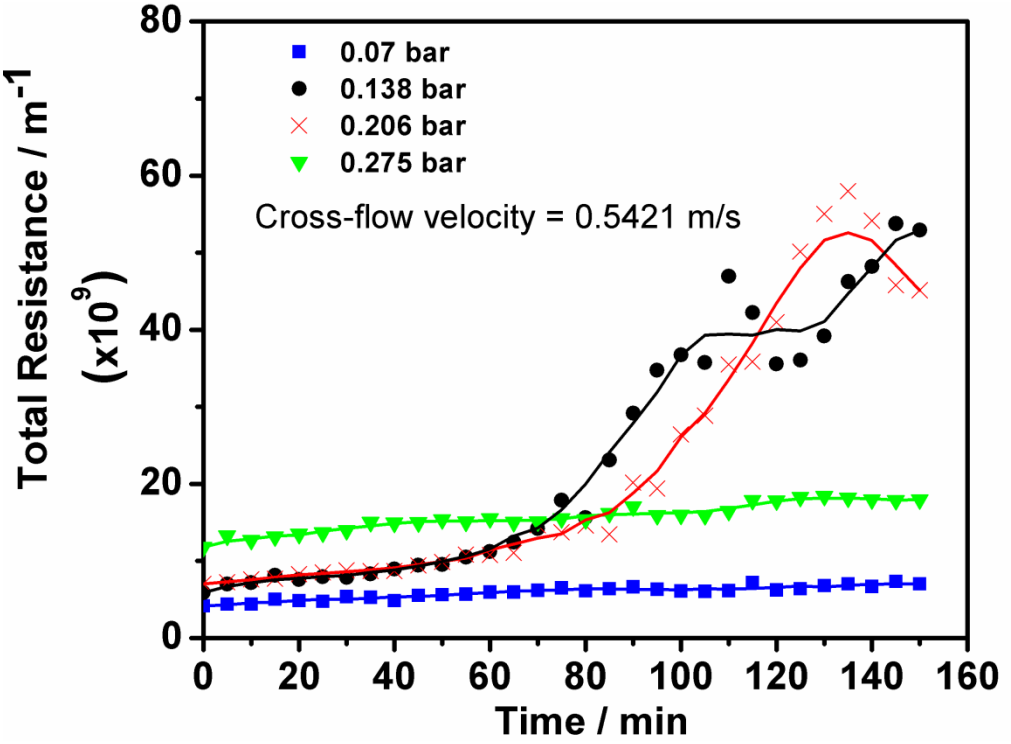

Figure 10. Total Resistance as a Function of Time for Membranes Operated at Various Pressures under Constant Cross-flow Velocity of 0.5421 m/s.

Figure 10 shows the total resistance curve of the membrane operated at different pressures while keeping the cross-flow velocity unchanged. At 0.07 bar, the resistance curve increase with a decreasing slope throughout the entire experiment and is concave down. This indicates that the membrane was fouled externally. However, as the pressure was increased to 0.138 bar, the resistance curves are changed. Initially, the resistance increases with an increasing slope (concave up) until to the point of inflection (at 100 min), beyond which the resistance increases with a decreasing slope (concave down). This shows that the fouling is governed by internal fouling followed by external fouling. It is postulated that, during the early stage, the water droplets deposit within the pores (but do not permeate across the membrane), causing a corresponding decline in pore volume. As a result, the

resistance rises rapidly. At approximately 100 min, most of the pores are blocked and the depositing droplets start to grow a layer on the membrane surface, engendering further increase in total resistance. During the surface deposition, it is likely that the water droplets aggregate into bigger droplets which serve as sites for further deposition. It is noticed that there is a sudden resistance decline at 110 min. This might be due to the unexpected escape of water droplets from the membrane pore as a result of scouring effect during the permeate collection. Hence, it caused a temporary drop of total resistance before the water droplet deposition site was quickly refilled. After 110 min, the fouling layer started building up which led to the rapid rise in total resistance. Similarly, at 0.206 bar, the membrane is initially fouled from within for the first 85 min and then the growth of cake layer on the membrane surface induce the external fouling. It appear that resistance decreases after it reaches the maximum resistance at 135 min. This may be due to the permeation of water droplets that originally clog the internal pores across the membrane. The water droplets found in the permeate when collected at 0.206 bar could support this hypothesis. Lastly, when the pressure is increased to 0.275 bar, only external fouling dominates. This is because the applied pressure is sufficient enough to push the water droplets through the membrane. Under such condition, it is unlikely for the water droplets to deposit in the pores and thus the internal resistance cannot be built up.

On the other side, it is noted that the resistance curves for water-oil separation operated at 0.07 and 0.275 bar are similar. Except that the cake layer buildup takes place immediately on the membrane surface, both exhibit very steady resistance over the operation time. This is due to the slow growth of cake layer. At low

pressure (0.07 bar), the liquefied cake layer could be scoured off whereas water droplets permeate through the membrane at high pressure (0.275 bar). Both situations do not favor the growth of cake layer and hence the resistance cannot be built up. However, it can be deduced that the cake layer thickness is larger at 0.275 bar than at 0.07 bar because the total resistance is greater at 0.275 bar. For 0.138 and 0.206 bar, the total resistance starts off lower but increases to 2-4 times the resistance at 0.07 and 0.275 bar by the end of runs. This is because the total resistance combines the resistance from both internal and external fouling.

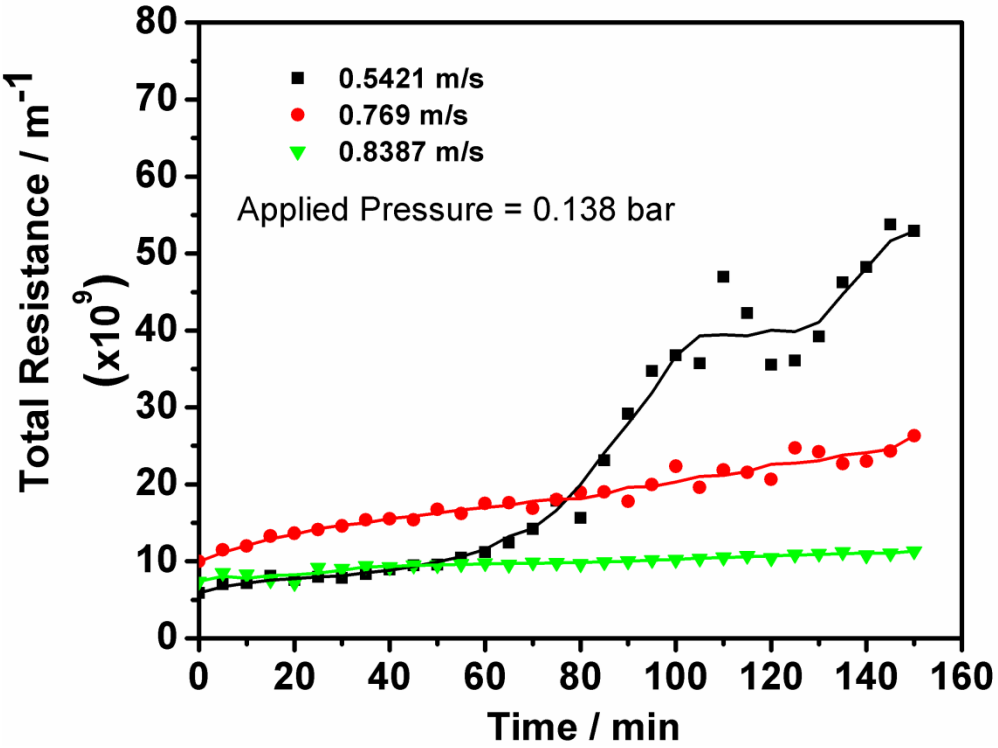

Figure 11. Total Resistance as a Function of Time for Membranes Operated at Various Cross-Flow Velocities under Constant Operating Pressure of 0.138 bar.

The effect of cross-flow velocity to the membrane fouling was also studied. Figure 11 shows the total resistance curve when the membrane was ran at 3 different cross-flow velocities. At 0.5421 m/s, the membrane fouling is a combination of internal

and external fouling. However, the external fouling prevails when the cross-flow velocity is increased to and above 0.769 m/s. At high cross-flow velocities while keeping relatively low pressure, the chance for the water droplets to clog the pores or accumulate on the membrane surface is lessened because the tangential feed flow traveling across the membrane surface will wash away the retained droplets. By that, the accumulation of cake layer can be mitigated or even eliminated. This can be manifested from the relatively low total resistance at 0.769 and 0.8387 m/s as compared to that at 0.5421 m/s. Furthermore, it is observed that the accumulation rate of cake layer is lower when a higher cross-flow velocity is applied. At 0.5421 m/s, the induced scouring effect is insignificant so that pore blocking can still take place.

4.6 Fitting of Membrane Fouling Models

To determine the model parameters, the fouling models are applied to the experimental data. For internal fouling, models for standard pore blocking and complete pore blocking are applied to the experimental data occurring before the point of inflection. However, for external fouling, cake filtration model is employed after point of inflection. For the cases in which cake filtration is deemed to be governing fouling mechanism for the entire time period, only cake filtration model is applied. Table 1 summarizes the values of fouling constants determined from the slopes, initial permeate flux determined from the intercepts together with the regression coefficients. Figures 12-14 show the fitting of each model to the data. Note that the regression of data in the figures was not performed for the entire

experiment although the dominant mechanism is deduced to be external fouling. This is owing to the fact that the rejection coefficient was not constant for earlier times. [28]

As seen in the table, cake filtration model fit the data very well with regression coefficient (r^2) greater than 99% for all cases. However, the initial flux obtained from the intercepts does not yield accurate values. This is simply because the cake filtration model applies at later times instead of initial times. Since K_3 is proportional to specific cake resistance according to $K_3=\mu C_3\rho/(2A^2\Delta P)$ where μ is solution viscosity, C_3 specific cake resistance, ρ the mass of cake deposited per volume filtrate, A membrane surface area and ΔP the transmembrane pressure (Belter, Cussler et al. 1987), a lower value of K_3 means that the specific cake resistance is lower. Among the various operating conditions, It is found that the membrane operated at 0.138 bar and 0.8387 m/s experiences from the least resistance resulted from cake filtration whereas the highest cake resistance is resulted when cross-flow velocity is 0.5421 m/s under the same applied pressure. In fact, K_3 decreases with increasing cross-flow velocity. As mentioned earlier, the plausible explanation can be the shear effect at high cross-flow velocity. These results are in good agreement with the total resistance data.

For cases in which internal and external fouling take effect, both complete and standard pore blocking models are applied to the data before the cake layer is developed. Compared to standard pore blocking model, complete pore blocking model appears to better fit the data because the regression coefficient is higher (> 90%). Furthermore, the initial fluxes determined from the complete blocking model

is closer to the experimentally measured data. These lead to the postulation that the water droplets deposit on instead of within the pores during the early stage.

Table 1. Internal and External Fouling Model Constants from Linear Regression of Filtration Data.

Cross-flow Velocity (ms^{-1})	Pressure (bar)	Initial Permeate Flux, J_o (L/m^2-hr)	Complete Blocking Model			Standard Blocking Model			Cake Filtration Model		
			Jo	K_1 (L^{-1})	R^2	Jo	K_2 (min^{-1})	R^2	Jo	K_3 (min/L^2)	R^2
0.5421	0.07	2014.3	N.A	N.A	N.A	N.A	N.A	N.A	420.2	13.3	0.99
0.5421	0.138	2817.3	2946.5	5.11	0.94	3258	3.85	0.85	-120.25	372.56	0.99
0.5421	0.206	3534.7	3865.7	5.404	0.91	3085	3.649	0.82	-98.51	353.89	0.99
0.5421	0.275	2796.1	N.A	N.A	N.A	N.A	N.A	N.A	197.4	50.38	0.99
0.769	0.138	1660.8	N.A	N.A	N.A	N.A	N.A	N.A	204.31	210.1	0.99
0.8387	0.138	2244.9	N.A	N.A	N.A	N.A	N.A	N.A	470.95	8.23	0.99

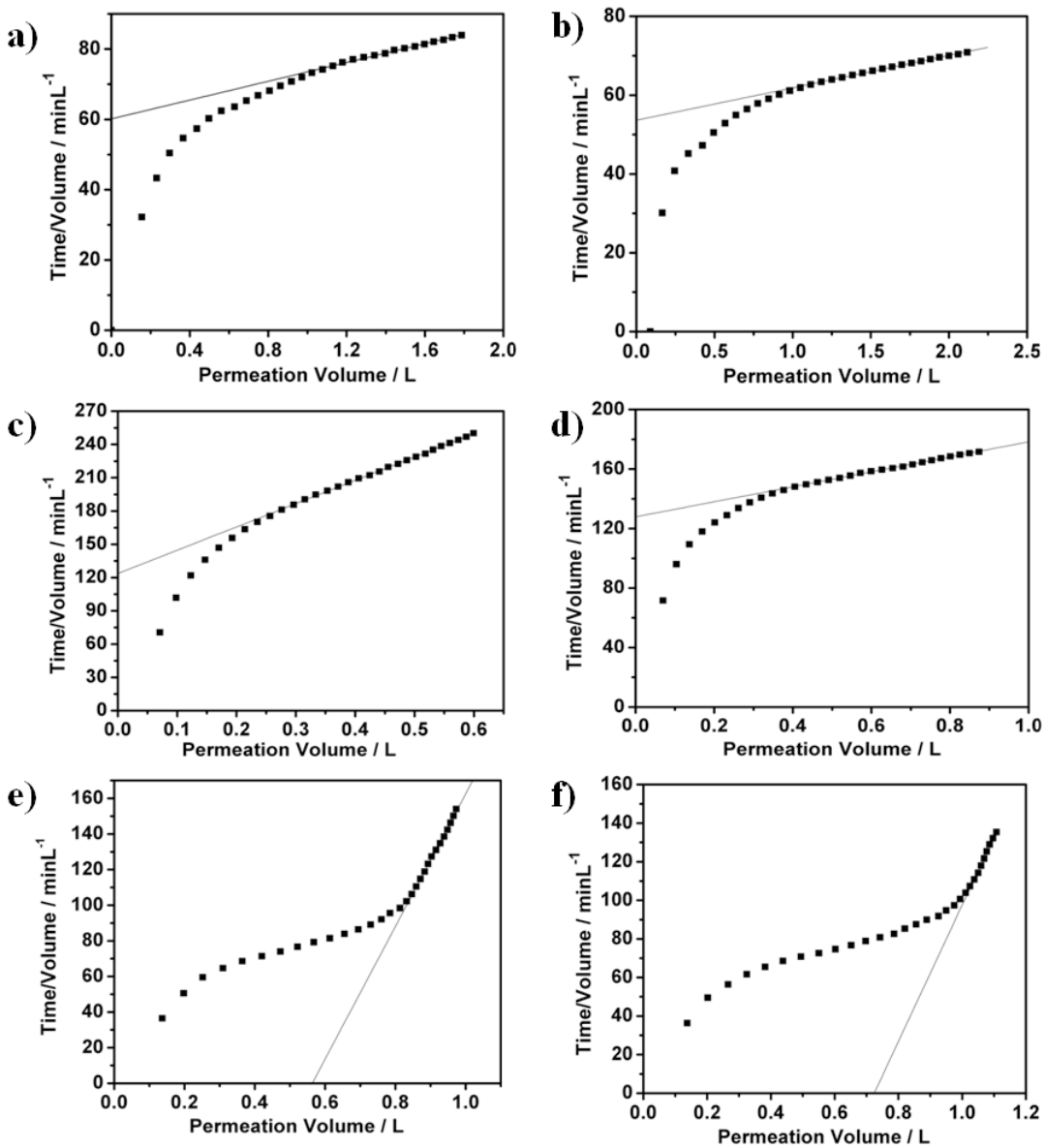

Figure 12. Cake Filtration Model Applied to Experimental Data for the Membrane Operated at a) 0.07 bar, 0.5421 m/s b) 0.138 bar, 0.8387 m/s c) 0.138 bar, 0.769 m/s d) 0.275 bar, 0.5421 m/s e) 0.138 bar, 0.5421 m/s and f) 0.206 bar, 0.5421 m/s.

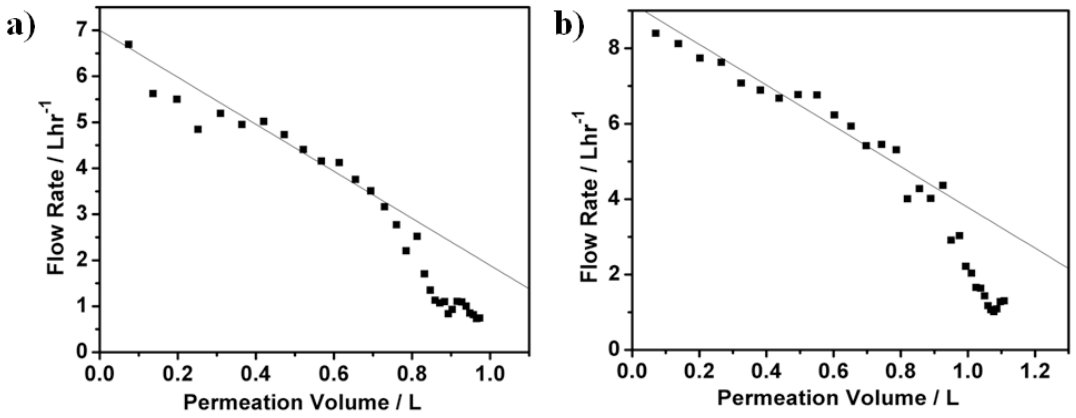

Figure 13. Complete Pore Blocking Model Applied to Experimental Data for the Membrane Operated at a) 00.138 bar, 0.5421 m/s and b) 0.206 bar, 0.5421 m/s.

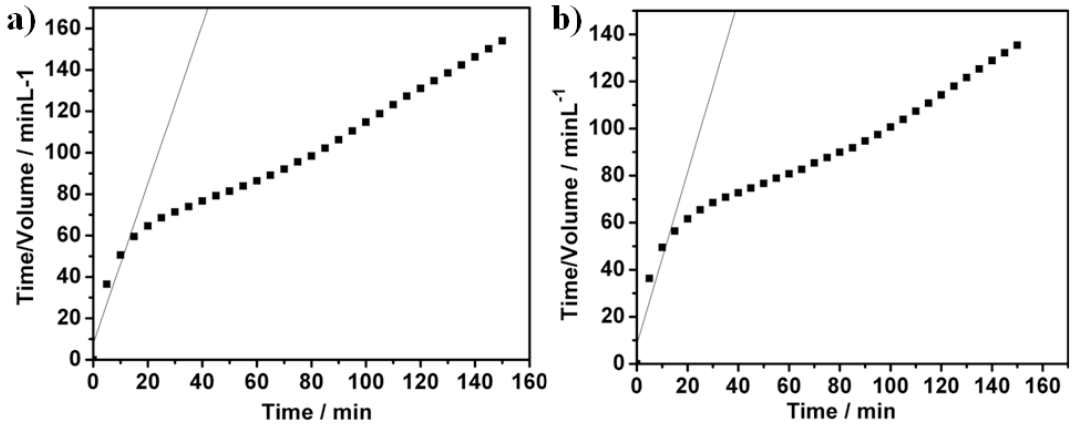

Figure 14. Standard Pore Blocking Model Applied to Experimental Data for the Membrane Operated at a) 00.138 bar, 0.5421 m/s and b) 0.206 bar, 0.5421 m/s.

4.7 Optimization of Operating Conditions

The collective effect of operating pressure and cross-flow velocity to the oil permeation is studied by constructing contour (Figure 15) which is useful for visual explanation and figuring out the optimum operating conditions. The color gradient clearly shows the

distribution of flux decline percentage as a function of both pressure and cross-flow velocity. Within the experimental data boundary, It can be seen that flux decline percentage decreases with increasing cross-flow velocity and applied pressure. A maximum flux decline (grey region) is resulted when a low cross-flow velocity and a considerably high pressure is employed. As discussed earlier, the reason for it is due to the accumulation of cake layer which exerts additional hydraulic resistance to the oil permeation. Therefore, it shall be avoided. By taking the grey region as a starting point, one can clearly see that both increasing and decreasing the pressure while holding the cross-flow velocity constant have a positive effect to the oil permeation. However, by taking the consideration that the pressure greater than 0.206 bar will leads to the undesirable penetration of water droplets across membrane and filtration ceases at pressure lower than 0.07 bar, hence the optimum operating conditions for efficient oil-water filtration shall be at high cross-flow velocity and low pressure (not smaller than 0.07 bar) which is located at the right bottom corner in the contour plot.

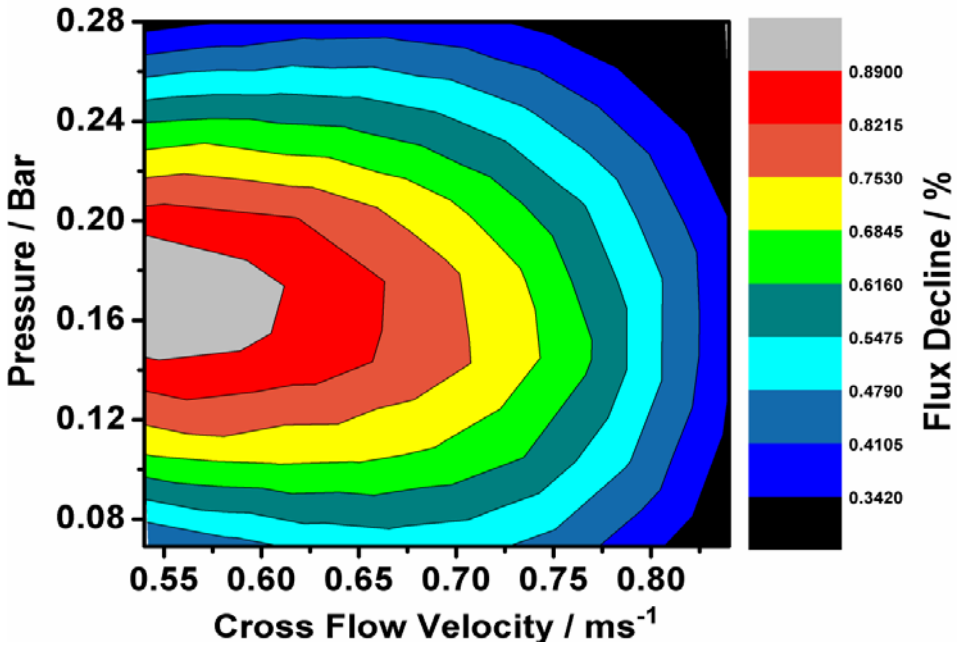

Figure 15. Contour Plot as a Function of Pressure, Cross-flow Velocity and Flux Decline Percentage.

5. Conclusions

With its unique interconnected pore structure, the electrospun carbon-silica nanofiber membrane enables water-oil separation at high flux under low pressure. High flux and low pressure imply higher energy efficiency and thus lower operating cost. Separation of water-in-oil emulsion was performed using the membrane and both the cross-flow velocity and operating pressure have direct influence to the flux and rejection efficiency. The effect of operating pressure to the final flux is dependent of the breakthrough pressure for oil as the cross-flow velocity is remained unchanged. A greater flux decline was resulted if the filtration was carried out at above the breakthrough pressure and vice versa. The analysis based on rejection efficiency suggests that the breakthrough pressure is higher than 0.206 bar. On the other side, the shear effect induced by cross-flow velocity mitigates the fouling problem by scouring off the foulant layer accumulated on the membrane surface. Therefore, flux decline is reduced. The scouring effect is also reflected in the reduction of specific cake resistance.

The membrane fouling models derived from Darcy's law can fit the experimental data with greater than 80% confidence level. Of the internal fouling model, complete pore blocking model offer a better fit than standard blocking model. However, whether a membrane is fouled internally, externally or both highly depends on the operating conditions. The optimization study indicates that the membrane achieves its optimum performance (in terms of flux decline in conjunction with rejection efficiency) at high cross-flow velocity and considerably low applied pressure.

Acknowledgement

Ming Hang is funded by the Singapore-Stanford Partnership Program. We would like to thank the lab technicians from Environment Lab and Central Environmental Science and Engineering (CESEL) lab in Nanyang Technological University (NTU) for technical support.

References

[1] T. Frising, C. Noïk, C. Dalmazzone, The Liquid/Liquid Sedimentation Process: From Droplet Coalescence to Technologically Enhanced Water/Oil Emulsion Gravity Separators: A Review, Journal of dispersion science and technology, 27 (2006) 1035-1057.
[2] J.A. Zeevalkink, J.J. Brunsmann, Oil removal from water in parallel plate gravity-type separators, Water Research, 17 (1983) 365-373.
[3] A.A. Al-Shamrani, A. James, H. Xiao, Destabilisation of oil–water emulsions and separation by dissolved air flotation, Water Research, 36 (2002) 1503-1512.
[4] N.D. Sylvester, J.J. Byeseda, Oil/water separation by induced-air flotation, Society of Petroleum Engineers Journal, 20 (1980) 579-590.
[5] J. Li, Y. Gu, Coalescence of oil-in-water emulsions in fibrous and granular beds, Separation and purification technology, 42 (2005) 1-13.
[6] L.A. Spielman, Y.-P. Su, Coalescence of Oil-in-Water Suspensions by Flow through Porous Media, Industrial & Engineering Chemistry Fundamentals, 16 (1977) 272-282.
[7] C.-F. Wang, F.-S. Tzeng, H.-G. Chen, C.-J. Chang, Ultraviolet-Durable Superhydrophobic Zinc Oxide-Coated Mesh Films for Surface and Underwater–Oil Capture and Transportation, Langmuir, 28 (2012) 10015-10019.
[8] F. Zhang, W.B. Zhang, Z. Shi, D. Wang, J. Jin, L. Jiang, Nanowire-Haired Inorganic Membranes with Superhydrophilicity and Underwater Ultralow Adhesive Superoleophobicity for High-Efficiency Oil/Water Separation, Advanced Materials, 25 (2013) 4192-4198.
[9] X. Li, D. Hu, K. Huang, C. Yang, Hierarchical Rough Surfaces Formed by LBL Self-assembly for Oil/Water Separation, Journal of Materials Chemistry A, (2014).
[10] J.A. Howarter, J.P. Youngblood, Amphiphile grafted membranes for the separation of oil-in-water dispersions, Journal of Colloid and Interface Science, 329 (2009) 127-132.
[11] N. Kocherginsky, C.L. Tan, W.F. Lu, Demulsification of water-in-oil emulsions via filtration through a hydrophilic polymer membrane, Journal of Membrane Science, 220 (2003) 117-128.
[12] M. Kukizaki, M. Goto, Demulsification of water-in-oil emulsions by permeation through Shirasu-porous-glass (SPG) membranes, Journal of Membrane Science, 322 (2008) 196-203.
[13] M. Tao, L. Xue, F. Liu, L. Jiang, An Intelligent Superwetting PVDF Membrane Showing Switchable Transport Performance for Oil/Water Separation, Advanced Materials, 26 (2014) 2943-2948.
[14] X. Gao, L.P. Xu, Z. Xue, L. Feng, J. Peng, Y. Wen, S. Wang, X. Zhang, Dual-Scaled Porous Nitrocellulose Membranes with Underwater Superoleophobicity for Highly Efficient Oil/Water Separation, Advanced Materials, 26 (2014) 1771-1775.
[15] W. Zhang, Z. Shi, F. Zhang, X. Liu, J. Jin, L. Jiang, Superhydrophobic and Superoleophilic PVDF Membranes for Effective Separation of Water-in-Oil Emulsions with High Flux, Advanced Materials, 25 (2013) 2071-2076.
[16] A. Koltuniewicz, R. Field, T. Arnot, Cross-flow and dead-end microfiltration of oily-water emulsion. Part I: Experimental study and analysis of flux decline, Journal of Membrane Science, 102 (1995) 193-207.
[17] K. Scott, R. Jachuck, D. Hall, Crossflow microfiltration of water-in-oil emulsions using corrugated membranes, Separation and purification technology, 22 (2001) 431-441.
[18] F.F. Nazzal, M.R. Wiesner, Microfiltration of oil-in-water emulsions, Water environment research, (1996) 1187-1191.
[19] P.-C. Chen, Z.-K. Xu, Mineral-Coated Polymer Membranes with Superhydrophilicity and Underwater Superoleophobicity for Effective Oil/Water Separation, Scientific reports, 3 (2013).
[20] J. Kong, K. Li, Oil removal from oil-in-water emulsions using PVDF membranes, Separation and purification technology, 16 (1999) 83-93.

[21] B. Chakrabarty, A. Ghoshal, M. Purkait, Ultrafiltration of stable oil-in-water emulsion by polysulfone membrane, Journal of Membrane Science, 325 (2008) 427-437.
[22] W. Chen, J. Peng, Y. Su, L. Zheng, L. Wang, Z. Jiang, Separation of oil/water emulsion using Pluronic F127 modified polyethersulfone ultrafiltration membranes, Separation and purification technology, 66 (2009) 591-597.
[23] M.W. Lee, S. An, S.S. Latthe, C. Lee, S. Hong, S.S. Yoon, Electrospun polystyrene nanofiber membrane with superhydrophobicity and superoleophilicity for selective separation of water and low viscous oil, ACS Applied Materials & Interfaces, 5 (2013) 10597-10604.
[24] R. Wang, Y. Liu, B. Li, B.S. Hsiao, B. Chu, Electrospun nanofibrous membranes for high flux microfiltration, Journal of Membrane Science, 392 (2012) 167-174.
[25] R. Gopal, S. Kaur, Z. Ma, C. Chan, S. Ramakrishna, T. Matsuura, Electrospun nanofibrous filtration membrane, Journal of Membrane Science, 281 (2006) 581-586.
[26] K. Yoon, K. Kim, X. Wang, D. Fang, B.S. Hsiao, B. Chu, High flux ultrafiltration membranes based on electrospun nanofibrous PAN scaffolds and chitosan coating, Polymer, 47 (2006) 2434-2441.
[27] X. Wang, X. Chen, K. Yoon, D. Fang, B.S. Hsiao, B. Chu, High flux filtration medium based on nanofibrous substrate with hydrophilic nanocomposite coating, Environmental Science & Technology, 39 (2005) 7684-7691.
[28] E.M. Tracey, R.H. Davis, Protein fouling of track-etched polycarbonate microfiltration membranes, Journal of Colloid and Interface Science, 167 (1994) 104-116.
[29] M.H. Tai, P. Gao, B.Y.L. Tan, D.D. Sun, J.O. Leckie, Highly Efficient and Flexible Electrospun Carbon–Silica Nanofibrous Membrane for Ultrafast Gravity-Driven Oil–Water Separation, ACS Applied Materials & Interfaces, 6 (2014) 9393-9401.
[30] K. Scott, A.J. Mahmood, R.J. Jachuck, B. Hu, Intensified membrane filtration with corrugated membranes, Journal of Membrane Science, 173 (2000) 1-16.
[31] B. Hu, K. Scott, Microfiltration of water in oil emulsions and evaluation of fouling mechanism, Chemical Engineering Journal, 136 (2008) 210-220.
[32] A. Ezzati, E. Gorouhi, T. Mohammadi, Separation of water in oil emulsions using microfiltration, Desalination, 185 (2005) 371-382.
[33] B. Hu, K. Scott, Influence of membrane material and corrugation and process conditions on emulsion microfiltration, Journal of Membrane Science, 294 (2007) 30-39.
[34] M. Zhang, L. Song, Mechanisms and Parameters Affecting Flux Decline in Cross-Flow Microfiltration and Ultrafiltration of Colloids, Environmental Science & Technology, 34 (2000) 3767-3773.
[35] T. Darvishzadeh, V.V. Tarabara, N.V. Priezjev, Oil droplet behavior at a pore entrance in the presence of crossflow: Implications for microfiltration of oil–water dispersions, Journal of Membrane Science, 447 (2013) 442-451.

Reviewers' comments:

Reviewer #1: This paper study the application of carbon-silica composite nanofiber membrane fabricated by electrospinning for oil purification from contained water. The effect of operation parameters; cross-flow velocity and pressure were studied as well as optimized. Membrane fouling mechanism was investigated with internal and external fouling models. COMMENTS:

(1)On method (page 9): "In order to maintain a constant concentration of the feed, the permeate was also recirculated to the feed thank". Please elaborate on how you performed this step because of the lack of expression in Fig. 1, and how you do this to avoid the interference of permeate measurement at the same time.

Thanks for pointing out the misleading part. Strictly, it is unlikely that the concentration of the feed is constant throughout the experiment because a part of water-oil emulsion would be trapped on the membrane surface and caused fouling. On the other hand, the permeate flux measurement was not continuous in the experiment. Instead, it was measured every 5 mins. The time to collect permeate ranged between 20s and 60s. Hence, the permeate recirculation does not affect the measurement. To avoid the confusion, we have rephrased the sentence in page 10, as follows:

"Both the permeate and retentate were pumped back to the feed tank. For permeate flux measurement, the permeate was collected in a beaker and weighed on a digital balance every 5 mins. The permeate collection time ranged between 20s and 60s. After that, the permeate was immediately transferred to the feed tank for recirculation."

(2)On method (page 10): "…the membrane was pre-coated with silicone oil via CVD. The coating was performed in oil bath at 140 ˚C for an hour". Please state the purpose of this step.

The purpose of this step is to increase the membrane's hydrophobicity. The sentence has been edited as follow

"…the membrane was pre-coated with silicone oil via CVD. The coating was performed in oil bath at 140 ˚C for an hour to increase the membrane's hydrophobicity".

(3)On discussion (page 12): "….. This makes the electrospun membrane a potential candidate for energy efficient treatment of waste oil". Please back up this claim with references of comparable technology commonly applied and their respective performance comparing to your result. The author should make a comparison with other membrane materials to clearly demonstrate the electrospun membrane as a "potential candidate".

Thanks for the suggestion. Four more references related to using membranes with structures and materials different electrospun carbon-silica membrane in crossflow filtration of water-

in-oil emulsion have been added in page 13 to support the claim. A comparison has also been made by giving an example.

(4)In figure 10, the authors fail to explain the difference between the resistance curve of P = 0.07 and 0.275 bar? It look like the total resistance of P = 0.07 and P = 0.275 bar is caused by the membrane itself. By the way, at p = 0.138 bar, the reasons about the result of resistance increase at t = 100 min and decrease at t = 110 min need to be addressed.

Thanks for the add-on. The difference between these two resistance curves lies on the initial resistance value. This is due to the inconsistency in membrane pore size. Such inconsistency stems from the limitation of electrospinning parameters to manipulate the membrane pore size and it also applies to the other two membranes (corresponding to curve of P=0.206 and P=0.138 bar) However, the variation of membrane pore size is slight because the initial resistance (at t = 0) of all four membranes started off at around $10x10^9$ m^{-1}.

Total resistance is the sum of membrane intrinsic resistance and fouling layer resistance. As seen in the figure 10, the total resistance of P=0.07 and P=0.275 bar are not constant over the 120 mins. The curves are instead increasing at slow rates. The reason is due to the slow growth of cake layer as explained in the main text. Therefore, the total resistance of P=0.07 and P=0.275 bar are contributed by the resistance from membrane itself as well as fouling layer formed on the membrane.

We have addressed the question related to the rise and drop in resistance between 100 - 110 min. A few sentences have been added in page 21 as follow:

"It is noticed that there is a resistance decline at 110 min. This might be due to the unexpected escape of water droplets from the membrane pore as a result of scouring effect during the permeate collection. Hence, it caused a temporary drop of total resistance before the water droplet deposition site was quickly refilled. After 110 min, the fouling layer started building up which led to the rise in total resistance."

(5)Some minor editing is needed to fix grammatical errors.

We have double checked the grammar and all spotted grammatical errors have been corrected.

Reviewer #2: The manuscript introduce the fabrication of carbon-silica electrospun membrane, which is applied to separate small volume water from the oil. The effects of two major operation parameters, transmembrane pressure and cross flow velocity are well studied. Fouling model is also investigated by applying experimental data to the various resistance models.

The idea is novel because no similar research has been conducted previously. However, the characterizations of electrospinning and membrane are not fully addressed, which can make

other researchers hard to follow up. Other issues, such as better clarification of some definitions, should be improved as well. For these reasons, this paper would be considered for publication after addressing the moderate comments listed below:

1. The duration of steady permeation flux is lower than 3 hours, therefore the performance might not be considered robust. Is it possible to obtain the data and analysis lasting longer than 5 hours?

Thanks for the suggestion. However, to obtain the data and analysis for filtration time greater than 5 hours, we need to start another round of experiment which is not feasible in this publication. In addition, there are many other journals report steady flux where the operation time lower than 3 hours. We aim to conduct a filtration test at longer time to study more affecting parameters in the future.

2. Page 7, additional electrospinning characterizations required: The tip-collection-distance, operation duration, temperature, humidity

The following sentences have been added in page 7:

"The electrospinning was performed at room temperature in a closed chamber where the electric field strength was sustained at approximately 0.6-0.8 kV/cm. The tip-collector distance was kept at 20 cm. To retard the hydrolysis of precursor, N_2 was purged from the side of spinneret during the electrospinning. At a solution feeding rate of 9-10 μl/min, 11-15 hours were required to electrospin the membrane."

3. Page 12, how does the bubble point analysis conduct? What is the experimental devices? How many tests have been run?

Thanks for the add-ons. To make clear of the experimental procedures, a new experimental section (section 3.2) was added in page 8.

4. Page 12, additional membrane characterizations required: SEM analysis, fibre distribution, thickness of membrane, contact angle. It is necessary to conduct these tests as we should know how the modification by carbon-silica affects the hydrophobicity and surface structure of the polymer membrane.

The detailed membrane characterizations and study of hydrophobicity have been done and published in the following journal which is cited as reference 29 in the manuscript:

M.H. Tai, P. Gao, B.Y.L. Tan, D.D. Sun, J.O. Leckie, Highly Efficient and Flexible Electrospun Carbon–Silica Nanofibrous Membrane for Ultrafast Gravity-Driven Oil–Water Separation, ACS Applied Materials & Interfaces, 6 (2014) 9393-9401.

5. Page 13, Fig 4 and Fig 6 is basically the same graph. The difference is that the set experiment in Fig 6 is conducted at cross-flow velocity of 0.5421 m/s, while Fig 4 has an unknown velocity. Fig 4 seems redundant.

Sorry for the misleading figures. In fact, Figure 4 and 6 are two different graphs. In Figure 4, the plot is flux of pure oil (without water droplets) against operating pressure. This is to primarily correlate the flux with the pressure and to demonstrate that high flux could be achieved under low pressure. On the other hand, the set experiment in Figure 6 is conducted using water-in-oil emulsion (instead of pure oil) to illustrate the effect of pressure to the flux under constant condition, i.e. cross-flow velocity, in this case.

To emphasize on the difference between the two figures, we have modified the sentence in page 14 while remaining Figure 4:

"Figure 6 shows variation of the initial permeate flux at applied pressure from 0.07 to 0.206 bar." into " Figure 6 shows variation of the initial permeate flux at applied pressure from 0.07 to 0.206 bar when water-in-oil emulsion was used."

6. Page 14, what is the definition of "steady flux"? In Fig 5, at the mentioned parameters, the permeate flux declined rapidly and reached nearly zero after 2 hour operation, how the steady flow considered as 370 LMH at the same conditions in Fig 7?

Thank you for pointing the mistake out. In the manuscript, the steady flux refers the final flux measured at the end of the filtration test. To avoid confusion, the use of "steady flux" has been removed and replaced with "final flux". On the other hand, Figure 5 and Figure 7 contradict each other. To eliminate contradiction, Figure 5 has been replaced with a figure plotted using the experimental data corresponding to the steady flow of 312 LMH as shown in Figure 7.

7. Fig 8, as mentioned in introduction, water might be dissolved in the oil which cannot be observed by naked eyes, therefore why the authors consider the optical microscopy image is adequate enough to assess the water rejection efficiency?

This is a good question. Under normal condition, water does not dissolve in oil due to the polarity dissimilarity. Water might "dissolve" in oil to produce emulsion provided that external force or power such as vigorous stirring and ultrosonication is applied. Even so, the emulsion is thermodynamically unstable system and will be readily destabilized through coalescence, creaming, sedimentation and etc. To form stable emulsion and with nanoscaled droplet size, use of emulsifiers (e.g. surfactants) and high-intensity ultrasound are required. Such emulsion can be lasted for days to weeks.

In our experiment, the water-in-oil emulsion was prepared without use of surfactant. In addition, the low-intensity ultrasonication was performed at mild stirring. Under such condition, the droplet size in the emulsion is much more likely at the micro-scale. On the

other hand, it was observed that the as-prepared emulsion was destabilized after 5-10 min. That is why the feed solution was replenished every 5 min during the filtration test. Therefore, it is not possible that the water will dissolve in the oil and forms emulsion whose sizes are beyond the detection limit of the optical microsocpe. This makes the optical microscopy image adequate enough to primarily assess the water rejection efficiency.

For clarification, more details have been added in the experimental section 3.3.

8. Page 18, why increasing the cross-flow velocity beyond 0.8387 m/s would result in the increased transmembrane pressure above 0.138 bar? Does it mean when velocity changes the applied pressure changes as well? Hence is there conflict between this assumption and Fig 9 which has fixed applied pressure of 0.138 bar?

In the experimental setup, only the transmembrane pressure was adjusted through throttling a valve. The cross-flow velocity was determined by taking the feed flowing rate at the applied pressure divided by the cross-sectional area of the feed channel spacer (which is the cross-sectional area of the tube in our experiment). Therefore, by varying the pressure, its corresponding cross-flow velocity can be calculated. In other words, cross-flow velocity is constant when the operating pressure is fixed. To avoid confusion, the sentences have been rephrased from

" It is noted that increasing the cross-flow velocity beyond 0.8387m/s is not feasible because the corresponding minimum pressure is above 0.138 bar which exceeds the hexadecane breakthrough pressure."

into

"It is noted that cross-flow velocity operated beyond 0.8387m/s is not feasible because the corresponding minimum pressure required is above 0.138 bar which exceeds the hexadecane breakthrough pressure."

The determination of cross-flow velocity has also been added into the experimental section in page 10 to make it more comprehensible.

9. As a novel fabrication concept, it is recommended that the authors to compare the permeation performance of the carbon-silica electrospun membrane with electrospun PAN membrane without modification, and commercial membranes also.

Thanks for the suggestion. By comparing the different membranes, the advantages of the carbon-silica electrospun membrane in term of water-oil emulsion permeation can be highlighted. However, one major difficulty encountered in the experiment was that the

unmodified electrospun PAN membrane is amphiphilic. Both water and oil can permeate through the membrane easily, rendering the permeation result less representative.

Therefore, instead of comparing all three types of membrane, several references have been cited to compare the permeation performance of the carbon-silica membrane with the reported commercial membranes (in page 13)

This work focuses on performance study and fouling mechanism of electrospun carbon-silica membrane. In future, we aim to study and compare the performance of carbon-silica membrane with other membranes from various perspectives.